PCCP

RSC Publishing

PAPER

View Article Online
View Journal | View Issue

Methane storage capabilities of diamond analogues†

Cite this: *Phys. Chem. Chem. Phys.*, 2013, **15**, 20937

Maciej Haranczyk,*[a] Li-Chiang Lin,[b] Kyuho Lee,[bc] Richard L. Martin,[a] Jeffrey B. Neaton[c] and Berend Smit[abd]

Received 7th September 2013,
Accepted 30th October 2013

DOI: 10.1039/c3cp53814a

www.rsc.org/pccp

Methane can be an alternative fuel for vehicular usage provided that new porous materials are developed for its efficient adsorption-based storage. Herein, we search for materials for this application within the family of diamond analogues. We used density functional theory to investigate structures in which tetrahedral C atoms of diamond are separated by –CC– or –BN– groups, as well as ones involving substitution of tetrahedral C atoms with Si and Ge atoms. The adsorptive and diffusive properties of methane are studied using classical molecular simulations. Our results suggest that the all-carbon structure has the highest volumetric methane uptake of 280 V_{STP}/V at p = 35 bar and T = 298 K. However, it suffers from limited methane diffusion. Alternatively, the considered Si and Ge-containing analogies have fast diffusive properties but their adsorption is lower, *ca.* 172–179 V_{STP}/V, at the same conditions.

1. Introduction

Natural gas, composed primarily (70–90%) of methane, is being investigated as a potential alternative fuel for vehicular usage due to its growing supply and lower CO_2 emissions comparing to traditional fuels. A critical step towards its widespread usage as a fuel for motor vehicles is to develop an on-board system that occupies about the same volume as a gasoline tank, and likewise stores enough natural gas to deliver about the same amount of energy. However the volumetric energy density of methane is relatively low (0.038 MJ L^{-1} methane at standard temperature and pressure, compared with 46.4 MJ L^{-1} for gasoline).[1] In order to minimize the size of the on-board natural gas storage system, the volumetric energy density of methane must be significantly increased. The US Department of Energy (DOE) set a target for a material's CH_4 uptake in this application: at external CH_4 pressure of 35 bar and temperature of 298 K, the material should hold at least 180 volumetric units of CH_4 at the standard temperature and pressure per unit volume of the material (V_{STP}/V). There are several approaches to accomplishing this: compression, liquefaction and adsorption on the surface of a porous material. The first two pose significant challenges due to safety and weight requirements on tank systems. The latter option poses challenges due to requirements on the porous material used for storage. There has been, however, tremendous progress made in this area, with many new classes of porous materials reported in recent years.

New classes of adsorbent materials include both crystalline materials such as metal–organic frameworks (MOFs),[2–4] and noncrystalline materials such as porous polymer networks[5] (PPNs, also porous aromatic frameworks[6] (PAFs)). MOFs are typified by crystalline coordination polymers comprising multitopic organic ligands bound to metal ions or metal ion clusters; the most notable members of this class of materials exhibit unprecedented levels of porosity as evidenced by relatively high surface areas (as high as 7100 m^2 g^{-1}),[7] and record-breaking gas sorption performance. However, MOFs have not yet been commercialized as natural gas sorbents due to their high cost and low chemical stability. PPNs are another class of porous materials that are being examined as potential methane sorbents. These materials are composed of covalently linked monomeric units that form tunable polymers exhibiting porosity.[8] For example, Zhou and co-workers at Texas A&M have developed a series of these porous polymers which exhibit superior chemical stability, and surface areas that approach those of some of the most porous MOFs.[5,8]

Determining the optimal structure of methane storage materials poses a significant challenge. It has to compromise two factors: on one hand the material needs to be highly porous (*e.g.* low density) to provide volume to store methane, on the other hand it needs adsorbent material (*e.g.* high density) that provides surface for the guest molecule to interact with and adsorb on. So far, identification of the optimal balance between these factors, that is identification of materials with high methane

[a] *Lawrence Berkeley National Laboratory, One Cyclotron Road, MS 50F-1650, Berkeley, CA 94720-8139, USA. E-mail: mharanczyk@lbl.gov; Fax: +1 510 486 5812; Tel: +1 510-486-7749*
[b] *Department of Chemical and Biomolecular Engineering, University of California, Berkeley, CA 94720, USA*
[c] *Molecular Foundry, Lawrence Berkeley National Laboratory, One Cyclotron Road, MS 50F-1650, Berkeley, CA 94720-8139, USA*
[d] *Department of Chemistry, University of California, Berkeley, CA 94720, USA*

† Electronic supplementary information (ESI) available. See DOI: 10.1039/c3cp53814a

storage capacity, has involved exhaustive or brute-force enumeration-and-screen strategies.[9] These methods are often expensive as they involve enumeration and analysis of large numbers of poorly performing materials; however, there has been progress in development of alternative approaches to the design of porous materials. For example, we have recently demonstrated a prototype of optimization-based design that allows blueprints of molecular building blocks that maximize either gravimetric[10] or volumetric[11] surface area of a porous material to be obtained. Our method demonstrated that, for example, porous materials of common topologies achieve the highest volumetric surface area when they are constructed from relatively simple, non-branched building blocks. Similarly, the idea of using such simple building blocks, *e.g.* alkyne (–CC–), to boost surface area was investigated by others.[12,13]

An example of successful tuning of methane uptake by (a) using alkyne groups to provide surface area and (b) the choice of a relatively dense framework topology to maximize methane–framework interaction comes from Huang and coworkers, who designed a new allotropy form of carbon: D-carbon.[14] The structure is an analogue of diamond in which all C–C bonds are expanded with alkyne groups (*i.e.* extended diamond). As a result, the distance between nodes of the diamond network is increased resulting in a porous framework that allows for possible use in methane storage applications. The predicted D-carbon structure was obtained using a planewave-based density function theory (DFT) approach. The uptake of methane was calculated using grand canonical Monte Carlo (GCMC) simulations with force-field parameters that were fitted to an experimental adsorption isotherm of the COF-102 structure,[15] which is a crystalline porous polymer with relatively similar chemistry. It was reported that D-carbon exhibits a record high excess volumetric methane uptake of 255 V_{STP}/V at 298 K and 35 bar, largely exceeding the DOE target value.

In the current study, we investigate the extended diamond structure as well as its analogues. Our DFT calculations consistently predict that the D-carbon structure has smaller pores than initially reported by Huang and coworkers,[14] affecting the material's performance in terms of both adsorption and diffusion. Herein, we note that the chemical makeup of the extended diamond structure can be further tuned. For porous polymers based on the diamond network, it is possible to exchange the tetrahedral carbon with Si or Ge atoms, *i.e.* PPN4 to PPN6 series reported by Zhou and co-workers.[5] Moreover, the alkyne group in extended diamond can be replaced with the isoelectronic –BN– group. In the following, we highlight our findings regarding methane adsorption and diffusion in extended diamond and its analogues.

2. Methods

We investigate the extended diamond structure using two systems: the orthogonal unit cell containing 40 atoms from Huang and coworkers[14] (denoted D-carbon) as well as a primitive unit cell with 10 atoms (denoted extDIA). Moreover, we consider analogues of extDIA, in which tetrahedral carbons are exchanged with Si and Ge. These structures are denoted as extDIA-Si and extDIA-Ge, respectively. The structures in which additional modifications are performed by exchanging the alkyne groups for –BN– groups are additionally marked with "BN". Fig. 1 illustrates extDIA and its analogues considered in this study.

For each of the considered structures, we have performed full geometry optimizations, including lattice vectors. Initial optimizations involved the periodic semi-empirical PM6 method implemented in Mopac2012,[16] followed by DFT. In DFT calculations, all atomic positions and lattice vectors are relaxed until the residual forces on every atom are smaller than 0.02 eV $Å^{-1}$ and the stress tensor components are smaller than 0.5 kbar using: (a) the Vienna *ab initio* simulation package (VASP) package[17] with the local density approximation (LDA)

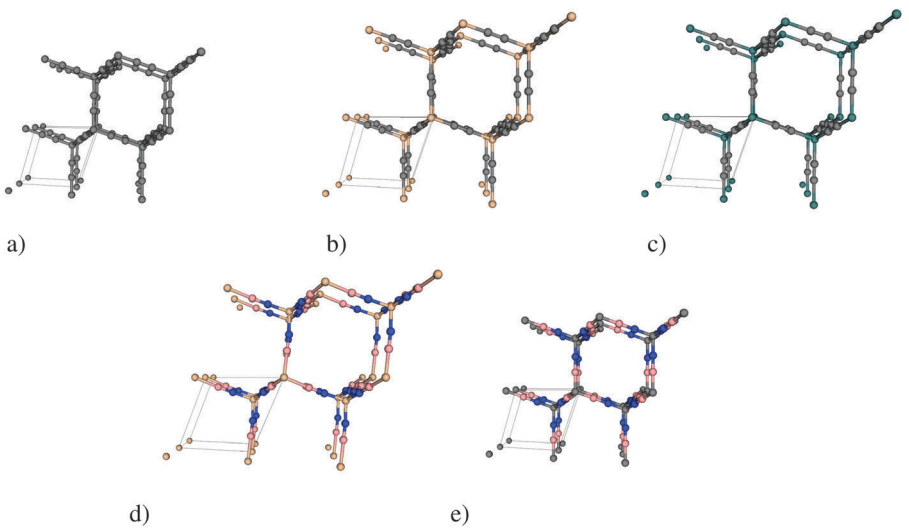

Fig. 1 The structures of extended diamond and its analogues considered in this study, shown to scale: (a) extDIA; (b) extDIA-Si; (c) extDIA-Ge; (d) extDIA-Si-BN; (e) extDIA-BN.

exchange–correlation functional, projector augmented wave (PAW)[18] potentials, and a 400 eV kinetic energy cutoff; and (b) Quantum ESPRESSO implementation[19] with the Perdew–Burke–Ernzerhof (PBE) exchange–correlation functional and Troullier–Martins type norm-conserving pseudopotentials with a 140 Rydberg kinetic energy cutoff. For all DFT calculations, a Γ-centered $2 \times 2 \times 2$ ($4 \times 4 \times 4$) k-point sampling for D-carbon (extDIA) is utilized. In addition, the structure of the (smaller) primitive unit cell, extDIA, was also optimized using the same criteria but with several different exchange–correlation functionals: LDA, PBE[20] and PW91[21] in VASP and LDA, PBE, PW91, PW92[22] in Quantum ESPRESSO.

Each of the optimized structures has been characterized in terms of the lattice parameters, the unit cell volume, the density of the material, and geometrical parameters describing the pores (diameters of the largest included (D_i) and free sphere (D_f) and helium void fraction (VF)). These parameters were calculated using Zeo++[23] with the high accuracy setting[24] and atomic radii adopted from the Cambridge Crystallographic Data Centre. A spherical probe of 1.2 Å radius has been used to simulate helium in the VF calculations.

Additionally, we have analyzed methane adsorption and diffusion properties using molecular simulations. In the simulations, the framework was regarded as rigid, and periodic boundary conditions were applied. The simulation box was composed of multiple unit cells with the distance in each perpendicular direction at least twice the cut-off radius (R_{cut} = 12.5 Å). The 12–6 Lennard-Jones potential model was adopted to describe the intermolecular interaction energies, in which we used the force field of ref. 14 for the framework atoms and the TraPPE model[25] for the methane molecule with the Lorentz–Berthelot mixing rule to predict all the pair-wise parameters. For each Monte Carlo simulation of adsorption, several million configurations through random translation, deletion, insertion, and regrow moves were sampled to obtain statistically accurate ensemble-averages. For each molecular dynamics simulation of diffusion, the canonical ensemble with Nose–Hoover thermostat was adopted. The simulation was performed at the infinite dilution condition of methane inside the framework. The time-step for updating each particle's position and velocity was chosen to be sufficiently small (*i.e.*, 0.5 fs) and the time span of each simulation was sufficiently long (*i.e.*, 100 ns). The self-diffusion coefficient was then obtained from analyzing the mean square displacement (MSD) computed from a collection of dynamics trajectories.[26]

3. Results

The relevant geometrical parameters describing the considered structures are summarized in Table 1. Additional information regarding the stability of the characterized species as well as performance of the semi-empirical PM6 method is placed in the ESI.† All of our DFT geometry relaxations for extended diamond have converged to very similar structures. The optimized unit cell volumes are within 3% difference and the corresponding densities are in the range 0.900–0.931 g cm^{-3}. The largest included sphere diameter (D_i) is between 4.34 and 4.44 Å while the free (restricting) sphere diameter (D_f) is between 3.40 and 3.48 Å, depending on the functional used. However, the optimized structures obtained in our study show some differences compared to the previously reported D-carbon structure.[14] The latter is a more open structure associated with a lower density of 0.83 g cm^{-3} and larger pores as indicated by values of D_i and D_f of 4.67 and 3.68 Å, respectively.

Table 1 Geometrical parameters describing the unit cells of the extended diamond structures and their void space: the unit cell parameters (a, b, c in Å and α, β, γ in degrees) and volume (UCV, in Å^3), helium accessible volume fraction (VF); largest included sphere diameter (D_i, in Å); largest free sphere diameter (D_f, in Å), and the corresponding materials' crystal density (d, in g cm^{-3}). The structures were obtained using different DFT exchange–correlation functionals, and the software packages utilized (VASP, Quantum Espresso(QE)) are also indicated after ''/'' separators

	a	b	c	α	β	γ	UCV	VF	D_i	D_f	d
D-carbon[a]	9.883	9.883	9.883	90.0	90.0	90.0	965.28	0.123	4.67	3.68	0.8265
D-carbon/LDA/VASP	9.515	9.515	9.515	90.0	90.0	90.0	861.55	0.094	4.37	3.42	0.9260
D-carbon/PBE/QE	9.598	9.598	9.598	90.0	90.0	90.0	884.18	0.100	4.44	3.48	0.9023
extDIA/PBE/VASP	6.806	6.764	6.819	59.780	59.535	59.931	220.68	0.100	4.42	3.46	0.9038
extDIA/LDA/VASP	6.762	6.703	6.778	59.679	59.354	59.857	215.42	0.094	4.35	3.40	0.9259
extDIA/PW91/VASP	6.802	6.765	6.814	59.810	59.587	59.949	220.62	0.100	4.42	3.46	0.9040
extDIA/PBE/QE	6.806	6.764	6.819	59.780	59.535	59.931	221.06	0.100	4.43	3.48	0.9022
extDIA/LDA/QE	6.776	6.778	6.779	60.074	60.011	60.096	220.51	0.100	4.43	3.47	0.9045
extDIA/PW91/QE	6.789	6.790	6.790	60.079	60.012	60.104	221.68	0.101	4.44	3.48	0.8997
extDIA/PW92/QE	6.712	6.713	6.713	60.074	60.012	60.096	214.16	0.092	4.34	3.41	0.9313
extDIA-Si/PBE/QE	7.932	7.944	7.936	59.938	59.946	59.961	353.13	0.226	5.53	4.61	0.7160
extDIA-Ge/PBE/QE	8.185	8.152	8.208	59.946	59.597	60.236	386.60	0.255	6.02	4.83	1.0365
extDIA-Si-BN/PBE/QE[b]	7.996	8.068	8.077	59.418	60.331	60.362	368.69	0.170	5.58	4.07	0.7001
extDIA-BN/PBE/QE[b]	6.861	6.853	6.859	60.120	59.911	60.062	228.20	0.053	4.31	2.95	0.8972

[a] Ref. 14. [b] Highest symmetry isomer was investigated.

We obtained, however, a 3.7% smaller lattice constant, a = 9.5157 Å, even if we started from the same unit cell structure as in ref. 14 and used the same LDA functional in VASP. Very tight convergence control parameters (*i.e.*, kinetic energy cutoff, *k*-point sampling, electronic convergence criterion and ionic convergence criterion up to 1000 eV, 7 × 7 × 7, 10^{-7} and 10^{-4}, respectively) produced essentially the same result. Also, our results from multiple functionals consistently predict structures with smaller pore diameters. In addition, we have further performed the calculation on the diamond structure with one of the investigated exchange–correlational functionals (*i.e.*, PBE). Our fully relaxed structure has the C–C bond length and density to be 1.542 Å and 3.535 g cm^{-3}, respectively, which are in excellent agreement with the experimentally reported data (*i.e.*, 1.545 Å and 3.516 g cm^{-3}).[27] Therefore, we may have confidence in the computed trends.

Nevertheless, it is important to note that from a DFT point of view these differences may look minor. It is very encouraging that two independent studies using different methods agree on the basic structure of these novel materials. What is surprising is that these differences in geometrical parameters describing the pore structure have drastic influences on the calculated adsorption and diffusion performance of the materials. To illustrate this effect, we perform classical molecular simulations on our extDIA structures optimized with the PBE functional. The resulting methane adsorption isotherms are presented in Fig. 2. The adsorption of CH_4 is higher in extDIA than in D-carbon at pressures higher than 10 bar, and it reaches 280 V_{STP}/V at 35 bar. Assuming methane release at 1 bar for vehicular applications, both extDIA and D-carbon structures would have the same working capacity of 241 V_{STP}/V. However, the extDIA structure exhibits a D_f 0.2 Å smaller than the 3.68 Å identified for D-carbon, suggesting possible limitations on the diffusion of methane molecules, whose kinetic diameter is *ca.* 3.85 Å. Indeed, we calculated the self-diffusion coefficient of methane at 298 K in extDIA to be 2.5 × 10^{-11} m^2 s^{-1}, an order of magnitude smaller than 3 × 10^{-10} m^2 s^{-1} obtained for D-carbon.

A possible strategy to increase methane diffusivity is to design an analogue of extDIA with slightly increased pore diameters. Substitution of the tetrahedral carbon with Si or Ge atoms leading to extDIA-Si and extDIA-Ge is considered. The structures of such analogues were relaxed using the PBE functional implemented in Quantum ESPRESSO. Their stability was confirmed by performing full phonon dispersion calculations, which is discussed in the ESI.† Molecular simulations of methane adsorption and diffusion were performed, adopting Dreiding force field parameters[28] for all elements not present in the extended diamond structure of ref. 14. The resulting materials indeed exhibit larger pores than extDIA, characterized by D_i of 5.53 and 6.02 Å and D_f of 4.61 and 4.83 Å for Si and Ge analogues of extDIA, respectively. Therefore, diffusion of methane is shown to be less restricted in these materials than in extDIA. The self-diffusion coefficients for methane are 1.6 × 10^{-8} and 2.5 × 10^{-8} m^2 s^{-1} for extDIA-Si and extDIA-Ge, respectively. Unfortunately, the opening of pores also decreases the methane adsorption at pressures higher than *ca.* 6 bar. The methane adsorption at 298 K and 35 bar is 172 and 174 V_{STP}/V for, respectively, extDIA-Si and extDIA-Ge. Moreover, the working capacity is much lower than for the extDIA structure, 138 and 144 V_{STP}/V, respectively. Apparently, the opening of pores by using larger tetrahedral atoms in extDIA-Si and extDIA-Ge was too extensive.

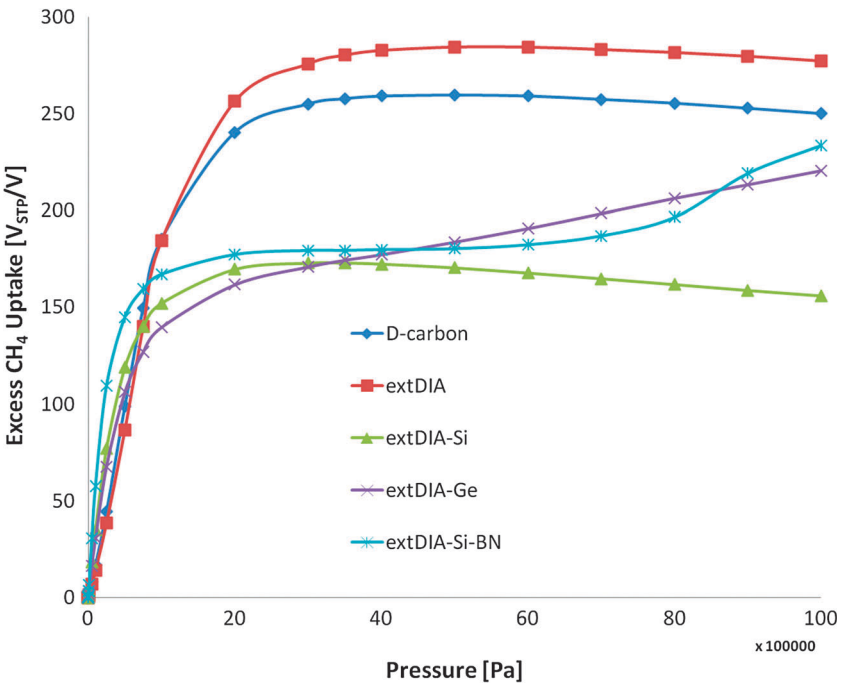

Fig. 2 The predicted excess methane adsorption isotherms obtained for the D-carbon structure of ref. 14, the extDIA structure, and its analogues. All structures are obtained using the PBE functional implemented in the Quantum Espresso software package.

In order to mitigate these negative impacts on adsorption performance in extDIA-Si and extDIA-Ge, we have investigated another analogue of extDIA-Si. Here, the pore size is reduced by replacing the –CC– alkyl group with a shorter isoelectronic –BN– group (Table 1). This change is shown to lead to the extDIA-Si-BN structure exhibiting methane uptake of 179 V_{STP}/V at 298 K and 35 bar, nearly meeting the ARPA-E target of 180 V_{STP}/V. However, this structure has a much lower working capacity of 122 V_{STP}/V. The self-diffusion coefficient for methane in extDIA-Si-BN is 1.7×10^{-8} m^2 s^{-1}, which is comparable to that of extDIA-Si exhibiting a D_f 0.6 Å smaller. Finally, we have also investigated a carbon-based analogue of extDIA-Si-BN, extDIA-BN. The latter structure, however, exhibits a D_f too small (2.93 Å) to permit diffusion of methane.

4. Conclusions

We have searched for materials for vehicular methane storage application within the family of diamond analogues. We used density functional theory and the semi-empirical PM6 method to investigate structures in which tetrahedral C atoms of diamond are separated by –CC– or –BN– groups, as well as ones involving substitution of tetrahedral C atoms with Si and Ge atoms. The materials' methane adsorption and diffusion properties have been studied using classical Monte Carlo and molecular dynamics simulations, respectively. Our results suggest that the all-carbon structure has the highest volumetric methane uptake at 280 V_{STP}/V at $p = 35$ bar and $T = 298$ K outperforming the most promising MOF materials by *ca.* 35%.[29] However, it suffers from limited methane diffusion. The considered Si and Ge-containing analogues do not suffer from such diffusion limitations, however their adsorption is shown to be lower, *ca.* 172–179 V_{STP}/V, at the same conditions.

Acknowledgements

The authors would like to thank Dr James Stewart for providing the MOPAC license. M.H. and R.L.M. were supported by ARPA-E MOVE program under Award Number DE-AR0000249 while L.-C.L., K.L., and B.S. were supported by the U.S. Department of Energy, Office of Basic Energy Sciences, Division of Chemical Sciences, Geosciences and Biosciences under Award DE-FG02-12ER16362. Portions of this work was done at the Lawrence Berkeley National Laboratory and at the Molecular Foundry, which are supported by the Office of Science, Office of Basic Energy Sciences, of the U.S. Department of Energy under Contract No. DE-AC02-05CH11231. This research used resources of the National Energy Research Scientific Computing Center, which is supported by the Office of Science of the U.S. Department of Energy under Contract No. DE-AC02-05CH11231.

References

1 T. A. Makal, J.-R. Li, W. Lu and H.-C. Zhou, *Chem. Soc. Rev.*, 2012, **41**, 7761.
2 M. Eddaoudi, J. Kim, N. Rosi, D. Vodak, J. Wachter, M. O'Keeffe and O. M. Yaghi, *Science*, 2002, **295**, 469.
3 R. B. Getman, Y.-S. Bae, C. E. Wilmer and R. Q. Snurr, *Chem. Rev.*, 2011, **112**, 703.
4 H. Wu, J. M. Simmons, Y. Liu, C. M. Brown, X.-S. Wang, S. Ma, V. K. Peterson, P. D. Southon, C. J. Kepert, H.-C. Zhou, T. Yildirim and W. Zhou, *Chem.–Eur. J.*, 2010, **16**, 5205.
5 (*a*) W. Lu, D. Yuan, D. Zhao, C. I. Schilling, O. Plietzsch, T. Muller, S. Bräse, J. Guenther, J. Blümel, R. Krishna, Z. Li and H.-C. Zhou, *Chem. Mater.*, 2010, **22**, 5964; (*b*) D. Yuan, W. Lu, D. Zhao and H.-C. Zhou, *Adv. Mater.*, 2011, **23**, 3723.
6 (*a*) T. Ben, H. Ren, S. Q. Ma, D. P. Cao, J. H. Lan, X. F. Jing, W. C. Wang, J. Xu, F. Deng, J. M. Simmons, S. L. Qiu and G. S. Zhu, *Angew. Chem., Int. Ed.*, 2009, **48**, 9457; (*b*) J. Schmidt, M. Werner and A. Thomas, *Macromolecules*, 2009, **42**, 4426.
7 O. K. Farha, I. Eryazici, N. C. Jeong, B. G. Hauser, C. E. Wilmer, A. A. Sarjeant, R. Q. Snurr, S. T. Nguyen, A. Ö. Yazaydın and J. T. Hupp, *J. Am. Chem. Soc.*, 2012, **134**, 15016.
8 M. Wriedt, J. P. Sculley, A. A. Yakovenko, Y. Ma, G. J. Halder, P. B. Balbuena and H.-C. Zhou, *Angew. Chem., Int. Ed.*, 2012, **51**, 9804.
9 C. E. Wilmer, M. Leaf, C. Y. Lee, O. K. Farha, B. G. Hauser, J. T. Hupp and R. Q. Snurr, *Nat. Chem.*, 2012, **4**, 83.
10 R. L. Martin and M. Haranczyk, *Chem. Sci.*, 2013, **4**, 1781.
11 R. L. Martin and M. Haranczyk, *J. Chem. Theory Comput.*, 2013, **9**, 2816.
12 O. K. Farha, C. E. Wilmer, I. Eryazici, B. G. Hauser, P. A. Parilla, K. O'Neill, A. A. Sarjeant, S. T. Nguyen, R. Q. Snurr and J. T. Hupp, *J. Am. Chem. Soc.*, 2012, **134**, 9860.
13 L. Sarkisov, *Adv. Mater.*, 2012, **24**, 3130.
14 L. Huang, Z. Xiang and D. Cao, *J. Mater. Chem. A*, 2013, **1**, 3851.
15 J. L. Mendoza-Cortes, T. A. Pascal and W. A. Goddard III, *J. Phys. Chem. A*, 2011, **115**, 13852.
16 (*a*) J. J. P. Stewart, *J. Mol. Model.*, 2007, **13**, 1173; (*b*) M. Korth, M. Pitonak, J. Rezac and P. Hobza, *J. Chem. Theory Comput.*, 2010, **6**, 344.
17 G. Kresse and J. Furthmüller, *Phys. Rev. B: Condens. Matter Mater. Phys.*, 1996, **54**, 11169.
18 (*a*) P. E. Blochl, *Phys. Rev. B: Condens. Matter Mater. Phys.*, 1994, **50**, 17953; (*b*) G. Kresse and D. Joubert, *Phys. Rev. B: Condens. Matter Mater. Phys.*, 1999, **59**, 1758.
19 P. Giannozzi, S. Baroni, N. Bonini, M. Calandra, R. Car, C. Cavazzoni, D. Ceresoli, G. L. Chiarotti, M. Cococcioni, I. Dabo, A. Dal Corso, S. de Gironcoli, S. Fabris, G. Fratesi, R. Gebauer, U. Gerstmann, C. Gougoussis, A. Kokalj, M. Lazzeri, L. Martin-Samos, N. Marzari, F. Mauri, R. Mazzarello, S. Paolini, A. Pasquarello, L. Paulatto, C. Sbraccia, S. Scandolo, G. Sclauzero, A. P. Seitsonen, A. Smogunov, P. Umari and R. M. Wentzcovitch, *J. Phys.: Condens. Matter*, 2009, **21**, 395502.
20 J. P. Perdew, K. Burke and M. Ernzerhof, *Phys. Rev. Lett.*, 1996, **77**, 3865.
21 (*a*) J. P. Perdew, in *Electronic Structure of Solids '91*, ed. P. Ziesche and H. Eschrig, Akademie Verlag, Berlin, 1991;

(*b*) J. P. Perdew, J. A. Chevary, S. H. Vosko, K. A. Jackson, M. R. Pederson, D. J. Singh and C. Fiolhais, *Phys. Rev. B: Condens. Matter Mater. Phys.*, 1992, **46**, 6671.
22 J. P. Perdew and Y. Wang, *Phys. Rev. B: Condens. Matter Mater. Phys.*, 1992, **45**, 13244.
23 T. F. Willems, C. H. Rycroft, M. Kazi, J. C. Meza and M. Haranczyk, *Microporous Mesoporous Mater.*, 2012, **149**, 134.
24 M. Pinheiro, R. L. Martin, C. H. Rycroft and M. Haranczyk, *CrystEngComm*, 2013, **15**, 7531–7538.
25 J. J. Potoff and J. I. Siepmann, *AIChE J.*, 2001, **47**, 1676.
26 B. Smit and T. Maesen, *Chem. Rev.*, 2008, **108**, 4125.
27 Crystal Structures and Lattice Parameters of Allotropes of the Elements, in *CRC Handbook of Chemistry and Physics, 94th Edition (Internet Version 2014)*, ed. W. M. Haynes, CRC Press/Taylor and Francis, Boca Raton, FL.
28 S. L. Mayo, B. D. Olafson and W. A. Goddard III, *J. Phys. Chem.*, 1990, **94**, 8897.
29 Y. Peng, V. Krungleviciute, I. Eryazici, J. T. Hupp, O. K. Farha and T. Yildirim, *J. Am. Chem. Soc.*, 2013, **135**, 11887–11894.

